

Performance Evaluation of Quantum Cascaded Lasers through VisSim Modeling

Mohamed B. El_Mashade^(a), Imbaby I. Mahamoud^(b), & Mohamed S. El_Tokhy^(b)

^(a) Electrical Engineering Dept., Al Azhar University, Nasr City, Cairo, Egypt

^(b) Engineering Dept. NRC, EAEA, Inchas, Egypt

engtokhy@gmail.com

ABSTRACT

Our goal in this paper is to evaluate the performance of quantum cascaded lasers (QCL's). The tools that we are used are the VisSim technique along with the block diagram programming procedures. The benefits of using this modeling language are the simplicity of carrying out the performance's measurement through computer simulation instead of setting up a practical procedure which becomes expensive as well as the difficulty of its management. The implemented models can help designers and scientists to optimize their devices to meet their requirements.

Keywords: *Quantum Cascaded Lasers (QCLs), Modeling, Block Diagram Programming, Intersubband transitions.*

1. INTRODUCTION

Quantum Cascaded lasers (QCLs) are new light sources based on intersubband transitions in quantum wells (QWs) [1]. These devices emit at wavelengths covering most of the mid-infrared (MIR) and part of the far-infrared (FIR) electromagnetic spectrum [2]. The extension to the far-infrared range is of particular interest due to the lack of narrow-band, powerful, and compact sources in this wavelength range. However, it presents a formidable challenge related to physics issues and technical difficulties [3].

The advent of the quantum cascade lasers (QCLs) with emission wavelengths available in the infrared range from 3 μm through more than 100 μm opens up the possibility of exploiting infrared atmospheric transparency windows for free space optical communications [4-5], trace gas analysis for pollution monitoring, environmental sensing, medical diagnostics, automobile applications military applications and wireless optical communications [6].

Additionally, the trend in the world was directed towards the quantum cascaded lasers because they have a several advantages over conventional laser diode, such as their high speed digital modulation and results on MIR optical wireless communication links, which demonstrate the possibility of reliably transmitting complex multimedia data streams [7].

Experimental Setups for measuring the characteristics of QCLs are reported [8]. However it is shown

difficulties in tuning and cost much. In this work block diagram technique is used to overcome the above mentioned complexity. Models are designed for the transport process, and carrier densities for QCLs devices. In this paper, the tunneling transition and population inversion are discussed in details. We focused here on improving the characteristics of QCLs, by exploiting the parameters that have a large effect on the performance of QCLs through our developed models. In this paper, the operational principles of quantum cascaded lasers were presented. To build a self-sustained oscillator like a laser, so, it is important that the condition of population inversion is satisfied. Block diagram models are implemented by ViSsim describing the lasing characteristics of QCLs. This paper is organized as follows: In section 2, we present the basic assumptions and model description. Proposed Simulator for Quantum Cascaded Laser including Tunneling process within QCLs model, and Population inversion model are considered in section 3. We summarize our results in section 4. Section 5 is devoted for conclusion.

2. BASIC ASSUMPTIONS AND MODEL DESCRIPTION

QCLs under consideration are complex devices, whose core is a multiple quantum wells (MQWs) [9]. Basically, QCLs containing a series of repeated InGaAs wells sandwiched between much thicker layers of the alloy semiconductor InAlAs barriers. But research has been expanded to other material systems, ultra-high-speed operation, and the exploration of different frequency ranges [10].

We assume that each quantum well (QW) contains three subband levels. The transitions between these subband levels are at equilibrium in the case of no bias and reach the flat condition, when the correct bias is applied [11]. It is assumed that the thermal effect of mobile carriers and thermally populated injector states of energy width are neglected. For the purpose of comparison, the QCLs parameters are chosen in such a way that they are compatible with the experimental ones.

As [10], the device realized by InGaAs/InAlAs lattice matched to InP, is constituted by one basic structure, which is known as a period, and this period is repeated several times. Each period is composed of two regions:

active region and relaxation-injection region. In the active region, the optical transition occurs and in the other one, the carriers can relax after having completed the optical transition. Since the injector region is highly doped, it can be acting as an electron reservoir and in turn it reinjects the electrons to the next period. This construction allows the electron to be recycling. Additionally, the injected carriers from the injector region; owing to resonant tunneling, to the upper lasing state of the active region, state $|3\rangle$, they can relax to state $|2\rangle$ by means of photon-assisted tunneling or by scattering. This scattering is mainly due to longitudinal (LO) phonon, given that $E_{32} \geq \hbar\omega_{LO}$ is satisfied. In the proposed model, the diagonal transitions are described by using three quantum wells. The Injector region contains five symmetrical QWs. The excitation energy between states 2 and 1 in each QW is assumed to be comparable with the phonon energy ($\sim 36\text{meV}$). The applied biasing voltage should be sufficient to cause a tunneling into QCLs. In most cases of QCLs, the characteristic temperature " T_0 " depends on the chosen compound material. QCLs has the advantage of a large T_0 that allows it to operate at higher temperature [12].

3. PROPOSED MODELS FOR QUANTUM CASCADED LASERS

Proposed programs for modeling and simulation of QCLs behavior is partially implemented in VisSim environment. VisSim is a visual block diagram for nonlinear dynamic simulation. The basic part of this diagram is based on what is known as a block. This block allows users to create their corresponding one in C/C++. In this environment, the system is modeled by the graphical interconnection of function blocks. For flexibility, variables are used to denote system parameters and then are assigned values in a separate compound blocks. Once the underlined problem was represented by its group of blocks, it is ready to be evaluated through the VisSim which is internally programmed. The program can be distributed with VisSim viewer or through generated C code from VisSim block diagram, which means that it doesn't depend on the VisSim environment [13].

3.1. Tunneling Process within QCLs Model

Block diagram modeling technique is used to represent the basic equation of tunnelling current derived by Kazarinov and Suris. The developed model is used to study the effect of current on both tunneling rate and splitting energy. This allows detection of the minimal biasing current which produces tunnelling while in the same time reduces such splitting energy.

3.1.1. Resonant Tunneling

The resonant tunneling of the electrons between the ground state of the injector and the upper lasing state of the active region was derived by Kazarinov and suris [14] is expressed as follows:

$$J_{\max} = eN_s \frac{2\Omega_{13}^2 \tau_p}{1 + \Delta^2 \tau_p^2 + 4|\Omega_{13}|^2 \tau_p \tau_3} \quad (1)$$

$$\hbar\Delta = E_1(F) - E_{33}(F) = qd(F - F_r) \quad (2)$$

$$d = |Z_{gg} - Z_{33}| \quad (3)$$

here J_{\max} , e , N_s , τ_3 , τ_p , $2\Omega_{13}^2 \tau_p$, $\hbar\Delta$, d , F , and F_r denotes the maximum injected current, the electron charge, the sheet carrier density, the upper state life time, the in-plane dephasing time, the tunneling rate, the energy detuning from resonance, the spatial separation between the centroids of the two wavefunctions, the average electric field applied over the distance d and the electric field which brings the upper lasing state 3 and the ground state g of the injector into resonance respectively. Block diagram model describing the maximum current with the tunneling transport is depicted in Fig.(1).

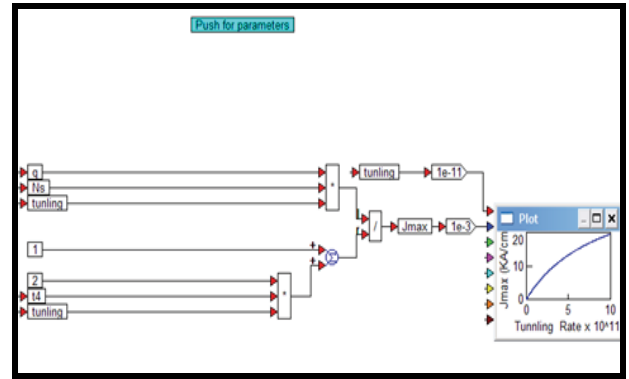


Figure 1: Model of Tunneling Rate and Maximum Current Density.

3.1.2. Splitting Energy and coupling parameters

The splitting energy ($2 \hbar\Omega_{13}$), between the two concerned states (ground state of the injector and the upper lasing state of the active region) and the J_{\max} , is described by the following relation that derived from Eq.(1) after simple calculation.

$$J_{\max} = \frac{q N_s S^2 \tau_p}{\frac{\hbar^2}{2\pi^2} + 2S^2 \tau_p \tau_3} \quad (4)$$

$S = 2 \hbar\Omega_{13}$ is the splitting energy. Block diagram model describing the maximum current with the splitting energy is depicted in Fig. (2).

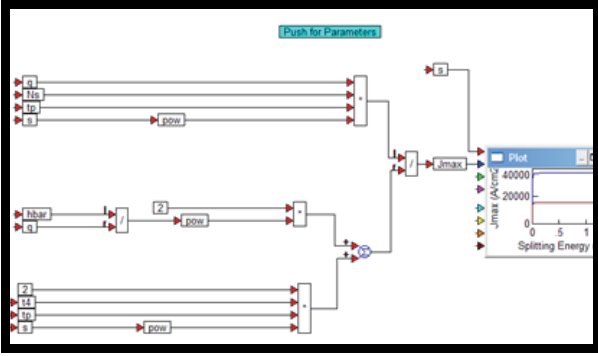


Figure 2: Block Diagram Model Of Splitting Energy And Maximum Current Density.

3.2. Population inversion model

A model for the bias current and carriers densities in quantum cascaded laser is presented. The non-linear rate equations for the electron densities, as a function of photon density, can be written as [8].

$$\frac{dn_3}{dt} = \frac{J_{in}}{q} - \frac{n_3}{\tau_{32}} - \frac{n_3}{\tau_{31}} - \Gamma v_g a (n_3 - n_2) (S_p + \frac{n_{sp}}{WL}) \quad (5)$$

$$\frac{dn_2}{dt} = \frac{n_3}{\tau_{32}} - \frac{n_2}{\tau_{21}} + \Gamma v_g a (n_3 - n_2) (S_p + \frac{n_{sp}}{WL}) \quad (6)$$

In the above expression, L , v_g , a , Γ , n_{sp} , n_3 & n_2 , S_p , τ_{32} , τ_{31} , and τ_{21} , denotes the length of the cavity, group velocity of the lasing modes, the differential gain (cm) contributed by a single gain stage, the mode confinement factor for the gain stage, the spontaneous emission factor, are the carrier densities in subbands 3 and 2, the photon density per unit width inside the optical cavity, the relaxation time of the optical transition of the electron between the states (3 and 2), the life time of the optical transition of the electron between the states (3 and 1) and the life time of the optical transition of the electron between the states (2 and 1), respectively. Block diagram model describes the effect of population inversion in QCLs system and its inherent operation are shown in Fig.(3).

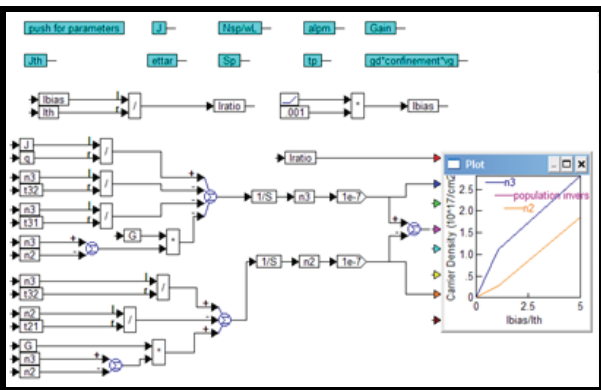


Figure 3: The Basic Model Describing the Rate Equations of Qcls.

4. SIMULATION RESULTS AND DISCUSSION

In this section, the results obtained from our developed models are presented. Our starting point of view is the relation between the tunneling rate and J_{max} , at different doping densities. Fig (4) depicts the plotting of the biasing current and the tunneling rate as a function of doping levels. It is noted that the alignment between the injector and the active regions improves as the current increases. This means that the splitting energy between the upper state of the active region and the ground state in the injector region decreases. As a result of this, a channel for the electrons will be created between the two concerned states and consequently the tunneling rate becomes higher. As a conclusion from the results of this figure, we can enhance the tunneling rate by changing some of other important parameters such as doping. As the doping increases, the required maximum current increases. This in turn will lead for the tunneling rate to become higher than before.

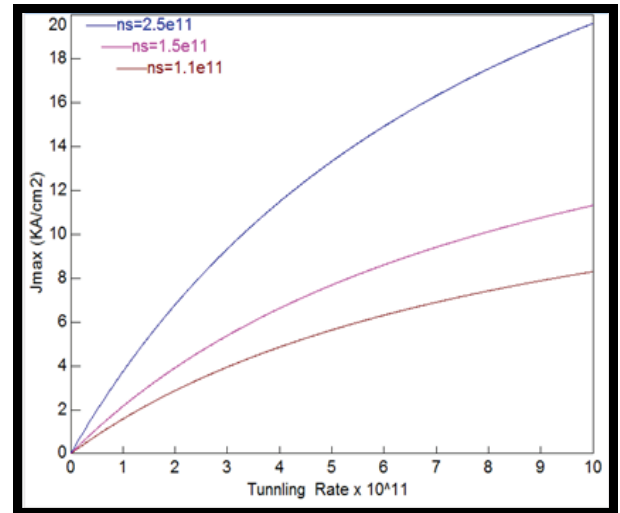


Figure 4: Variation of the Maximum Injected Current as a Function of the Tunneling Rate at Different Doping Levels.

Splitting energy ($2 \Omega_{ij} \hbar$) between the two concerned states (ground state of the injector and the upper lasing state of the active region), as a function of the maximum current density is depicted in Fig. (5). Since the splitting energy of the concerned states is increased, a large value of the current will be needed to compensate for the difference in energy between these two states. At the same time, two regions can be identified in the curve: one of them, which is characterized by the smallest splitting energy, the injection is very efficient and J_{max} is increased to balance the difference in energy between the two concerned states. In the second region, if the splitting energy increases above a certain limit, the injection current has no effect on it. This means that the injected current is not sufficient to make the two states near to one another. To overcome this difficulty, the doping effect must be used. As the doping increases, the carriers that transport to the active region will be increased. Consequently, higher performance of the

device is obtained. It is of importance to note that as the coupling becomes stronger, the fastest injection of carriers to the upper state of the laser transition can be achieved and this in turn makes the lasing action more flexible.

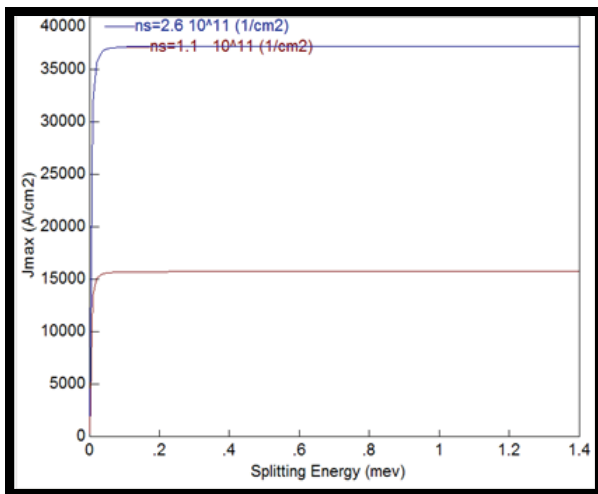


Figure 5: Splitting Energy As a Function of the Maximum Injected Current Parametric In Doping Density.

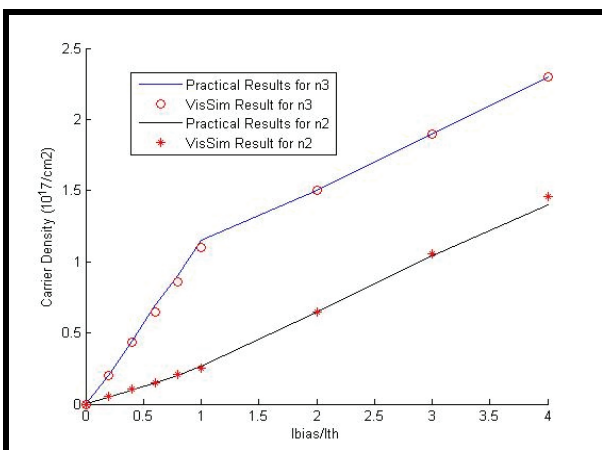


Figure 6: Variation of the Carrier Densities Along With the Population Inversion as a Function of the Bias Current.

We noticed that to enhance the capabilities of the system, doping of the injector region is necessary to maintain a steady-state population inversion as dictated by charge neutrality. And the level of doping must be carefully optimized to give minimal absorption and leakage.

The rate of change of electron densities in levels 3 and 2 with the bias current is shown in Fig.(6). From this figure, as the electrical current increases, the number of electrons in the upper subband increases and this in turn leads to enhance the population inversion. As a consequence of this, the number of photons will be raised and the lasing characteristics will be improved. The results of the underlined figure exhibit a bending at threshold. After threshold the carrier densities will be further increased with current. For this reason each

curve contains two lines with different slopes. These bendings in the rate of increasing of electron densities, with the bias current, result in discontinuities in the values of the differential resistance of the laser at threshold. Additionally, this behavior of theoretical results is in a good agreement with that published in [8].

At resonance, all electrons between the injector ground state and the upper laser state are equally distributed. While below resonance, the carriers reside in the upper laser state 3 is small compared to that state above threshold as Fig. (7) demonstrates. Below threshold, the carriers in subband n_2 are larger than that above threshold. This is because the carriers above threshold don't attain in this state. The energy of the electron is made equal to the phonon energy (the main scattering mechanism). So, there is a fast decay in this state for electrons as depicted in Fig.(7). Even though, the gain is clamped at its value which it attains at threshold. In the same time, the electron densities are continuously increasing with the bias current. As a result, an increase in the injected current density in QCLs does not only lead to an increase in the photon emission rate but it also leads to an increase in the rate of non-radiative transitions. Therefore, QCLs tend to have radiative efficiencies η_r significantly smaller than unity.

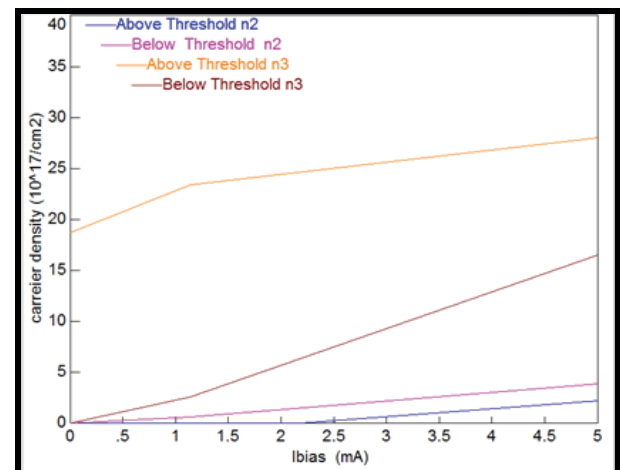


Figure 7: Dependent of the Carrier Densities On The Lasing State Above And Below Threshold.

Also, Figs.(7) shows that the population is much more widely distributed over the different levels below threshold. Also, above threshold, the carrier density in the quantum wells is strongly damped, and only the carrier density in the separate confinement heterostructure region provides negative feedback to suppress the noise associated with carrier injection.

5. CONCLUSION

In this work, models describing the performance of QCLs are developed. Block diagram programming technique is employed to implement these models. To ensure the validity of the model, comparison with the published practical result is performed. The models are used to study the effect of device parameters on

performance characteristics of the QCLs within user friendly graphical environment. Results show the effectiveness of methodology introduced. As an example, doping effect which received little attention in the literature is investigated.

REFERENCES

- L. A. Dunbar, V. Moreau, R. Ferrini and R. Houdr'e, 2005. Design, fabrication and optical characterization of quantum cascade lasers at terahertz frequencies using photonic crystal reflectors. *Optics Express*, 13(22), October.
- M. Razeghi, and S. Slivken, 2003. High powers quantum cascaded lasers grown by Gas MBE. *Opto-Electronics Review*, 11(2), pp. 85–91.
- R. Colombelli, F. Capasso, C. Gmachl, A. L. Hutchinson, D. L. Sivco, A. Tredicucci, M. C. Wanke, A. M. Sergent, and A. Y. Cho, 2001. Far-infrared surface-plasmon quantum-cascade lasers at 21.5 μm and 24 μm wavelengths. *Appl. Phys. Lett.*, 78(18), April .
- R. Martini and E.A. Whittaker, 2005. Quantum cascade laser-based free space optical communications. *Journal of Optical and Fiber Communications Reports*, 2(4), October.
- S. Blaser, D. Hofstetter, M. Beck and J. Faist, 2001. Free-space optical data link using Peltiercooled quantum cascade laser. *Electronics Letters*, 37(12), June.
- M. S. Taubman, T. L. Myers, B. D. Cannon, and R. M. Williams, F. Capasso, C. Gmachl, D. L. Sivco, and A. Y. Cho, 2002. Frequency stabilization of quantum-cascade lasers by use of optical cavities. *Optics Letters*, 27(24), December.
- F. Capasso, R. Paiella, R. Martini, R. Colombelli, C. Gmachl, T. L. Myers, M. S. Taubman, R. M. Williams, C. G. Bethea, K. Unterrainer, H. Y. Hwang, D. L. Sivco, A. Y. Cho, A. M. Sergent, H. C. Liu, and E. A. Whittaker, 2002. Quantum Cascade Lasers: Ultrahigh-Speed Operation, Optical Wireless Communication, Narrow Linewidth, and Far-Infrared Emission. *IEEE Journal of Quantum Electronics*, 38(6), June.
- Farhan Rana, Rajeev J. Ram, 2007. Theory of Current Noise and Photon Noise in Quantum Cascade Lasers. *arXiv:cond-mat/0108236v1 [cond-mat.mes-hall]*, July.
- Rita Claudia Iotti, and Fausto Rossi, 2001. Nature of Charge Transport in Quantum-Cascade Lasers. *Phys. Rev. Lett*, 87(14), October.
- F. Eickemeyer, 2005. *Ultrafast dynamics of coherent intersubband polarizations in quantum wells and quantum cascade laser structures*. Thesis (PhD). Neuchatel university.
- Markfox, 2001. Optical properties of solids. Oxford University, press, book, ch. 6.
- J. Faist, F. Capasso, Carlo Sirtori, Deborah L. Sivco, Albert L. Hutchinson, and Alfred Y. Cho, 1995. Vertical transition quantum cascade laser with Bragg confined excited state. *Appl. Phys. Lett.*, 66(5), January.
- H.M. Abdull-kader, A.B.El-Sisi, K.A. Mostafa, I I. Mahmoud, 2007. Implementation of A real-time Simulator for dynamic systems. *IJCI*, 1(1), July.
- T. Aellen, M. Beck, N. Hoyler, M. Giovannini, and J. Faist, 2006. Doping in quantum cascade lasers I. In AlAs–InGaAs/InP midinfrared devices. *Journal of Applied Physics*.